

1 **Scaleable production of microbubbles using an ultrasound-modulated microfluidic device**

2 Dario Carugo,^{1¶} Richard J. Browning,^{2¶} Ida Iranmanesh,² Walid Messaoudi,³ Paul Rademeyer,² and
3 Eleanor Stride^{2a}

4 ¹ *Department of Pharmaceutics, UCL School of Pharmacy, University College London (UCL), UK*

5 ² *Institute of Biomedical Engineering, Department of Engineering Science, University of Oxford, UK*

6 ³ *Faculty of Engineering and Physical Sciences, University of Southampton, UK*

7 [¶] *Authors have equally contributed to the work in this study*

8 Surfactant-coated gas microbubbles are widely used as contrast agents in ultrasound imaging and
9 increasingly in therapeutic applications. The response of microbubbles to ultrasound can be strongly
10 influenced by their size and coating properties and hence the production method. Ultrasonic
11 emulsification (sonication) is the most commonly employed method and can generate high
12 concentrations of microbubbles rapidly, but with a broad size distribution and there is a risk of
13 contamination and/or degradation of sensitive components. Microfluidic devices provide excellent
14 control over microbubble size, but are often challenging or costly to manufacture, offer low
15 production rates ($<10^6\text{s}^{-1}$), and are prone to clogging. In this study, a hybrid sonication-microfluidic
16 or ‘sonofluidic’ device was developed. Bubbles of $\sim 180\ \mu\text{m}$ diameter were produced rapidly in a T-
17 junction and subsequently exposed to ultrasound (71-73 kHz) within a microchannel, generating
18 microbubbles (mean diameter: 1-2 μm) at a rate of $>10^8\text{s}^{-1}$ using a single device. Microbubbles were
19 prepared using either the sonofluidic device or conventional sonication and their size, concentration
20 and stability compared. The mean diameter, concentration and stability were found to be
21 comparable between techniques, but the microbubbles produced by the sonofluidic device were all
22 $<5\ \mu\text{m}$ in diameter and thus did not require any post-production fractionation.

^a eleanor.stride@eng.ox.ac.uk

23 I. INTRODUCTION

24 A. Microbubbles in ultrasound imaging and therapy

25 In medical imaging, microbubbles are routinely used as ultrasound contrast agents. Their high
26 compressibility enables significant enhancement of ultrasound backscatter from blood by several
27 orders of magnitude. The microbubble core usually consists of a high molecular weight gas (e.g. a
28 perfluorocarbon or sulfur hexafluoride) stabilised by a surfactant or polymer coating (or “shell”) to
29 enhance stability during storage, handling, and/or administration (Stride and Saffari 2003). Typical
30 clinical formulations use saturated phospholipids or denatured albumin as the primary shell
31 constituents. Moreover, microbubbles can be loaded with biologically active compounds or
32 functionalised with targeting moieties. This has paved the way for their use as targetable drug delivery
33 systems, whereby the bioactive payload can be released on-demand upon extracorporeal ultrasound
34 stimulation directed to the point of treatment (Ferrara, et al. 2007, Kooiman, et al. 2014).

35 The clinical utility of microbubbles is profoundly influenced by their physical characteristics,
36 including their average size, size distribution, and the mechanical and rheological properties of the
37 coating layer (Alter, et al. 2009, Garg, et al. 2013, Sirsi, et al. 2010). These characteristics are in turn
38 dependent on the chemical formulation of the microbubble shell and also on the production technique
39 (Al-Jawadi and Thakur 2020, Hosny, et al. 2013). A variety of different methods have been developed
40 for batch production of microbubbles, including ultrasonic emulsification (sonication), high shear
41 emulsification, membrane emulsification, and coaxial electrohydrodynamic atomisation (Stride and
42 Edirisinghe 2008). Sonication is the most commonly employed method in both academic and
43 industrial laboratories, and involves dispersing gas or liquid in a suspension of a coating material using
44 high intensity ultrasound (Stride, et al. 2020). The size distribution of microbubbles obtained from
45 sonication is however relatively broad (Feshitan, et al. 2009) and there is also wide variability in coating
46 properties (Browning, et al. 2019), which may lead to a large variation in acoustic response across a

47 microbubble population (Rademeyer, et al. 2015). Post-production procedures (i.e., fractionation or
48 filtration) are usually required in order to remove large bubbles (i.e., with diameters $> 10 \mu\text{m}$) that
49 could cause vascular occlusion after intravenous injection, as well as excess coating material not
50 incorporated onto the microbubble (Dewitte, et al. 2019, Feshitan, et al. 2009). The latter is particularly
51 important in the case of drug-loaded microbubbles, to enable accurate quantification of the
52 administered dose.

53 **B. Microfluidic techniques for microbubble production**

54 More recently, microfluidic techniques have been proposed as an alternative to batch methods
55 for producing more uniform microbubbles (Chen, et al. 2014, Dhanaliwala, et al. 2013, Gnyawali, et
56 al. 2017, Hettiarachchi, et al. 2007, Jiang, et al. 2016, Peyman, et al. 2012, Rickel, et al. 2018, Segers, et
57 al. 2020, Seo, et al. 2010, van Elburg, et al. 2021). A typical microfluidic device consists of a cross-flow
58 (i.e., flow focusing) or T-junction architecture, in which gas and liquid streams are forced to flow into
59 a confined microchannel where the gas stream breaks up into individual microbubbles, a process often
60 referred to as ‘pinch-off’ (Garstecki, et al. 2006, Pahlavan, et al. 2019). Microbubbles produced with
61 this technique typically have a polydispersity index $< 5\%$. However, production of microbubbles
62 having clinically applicable diameters (i.e., in the range $1\text{-}10 \mu\text{m}$) requires microchannel features of
63 comparable dimensions (Hettiarachchi, et al. 2007), which can reduce a device’s lifetime considerably
64 (i.e., due to clogging or excessive backpressure). Depending on the geometrical properties of the
65 microchannels and the flow dynamic field, different microbubble production regimes have been
66 demonstrated using these architectures (Dollet, et al. 2008). However, production rates are typically
67 lower compared with batch methods (Table 1), and microbubble stability has also been reported to be
68 lower in some cases (Hosny, et al. 2013). These factors have hindered the adoption of microfluidics
69 for industrial production of microbubbles for clinical usage.

70 Some of these limitations can be addressed through changes to the operating conditions
71 and/or the device architecture. For example, Peyman *et al.* were able to achieve a micro-spraying
72 microbubble formation regime by varying the geometry of a flow-focusing microfluidic device,
73 specifically by widening the exit channel and introducing an abrupt increase in the channel depth.
74 When compared to a more conventional pinch-off formation regime, micro-spraying resulted in
75 microbubble suspensions having ~ 100 -times greater concentration (i.e., up to 10^9 microbubbles/mL)
76 (Peyman, et al. 2012). However, the size distribution of microbubbles produced by micro-spraying
77 presented comparable relative standard deviation to that of microbubbles produced by batch
78 mechanical agitation; although the latter method generated some microbubbles with diameter $>10 \mu\text{m}$
79 that were not present in the microfluidic-generated samples. Castro-Hernández *et al.* demonstrated
80 that careful selection of the hydrodynamic boundary conditions in a planar flow-focusing device can
81 enable production of microbubbles with dimensions one order of magnitude smaller than the
82 microchannel width, when the length of the exit channel is designed to be significantly greater than
83 its width (Castro-Hernández, et al. 2011). With this method, microbubbles $\sim 5 \mu\text{m}$ diameter and with
84 a polydispersity index $<5\%$ could be produced at a rate $>10^5$ microbubbles/sec, which represents an
85 improvement compared to more conventional microfluidic systems based on microbubble pinch-off.
86 However, manufacturing of the microchannels in this study still required costly and time-consuming
87 photolithographic techniques, and scaling up production of microbubble suspensions with a mean
88 diameter of $1\text{-}3 \mu\text{m}$ (often employed in therapeutic applications) could pose challenges.

89 Identifying a microbubble production method that relies on further scaled-up channel
90 architectures (i.e., up to 100s or 1000s of μm) would enable both greater production rates and
91 overcome challenges associated with clogging, high backpressure and manufacturing costs. However,
92 additional modifications to the microbubble production mechanism or the physico-chemical
93 properties of fluidic environment may be required in order to produce microbubbles of clinically

94 relevant sizes *via* these scaled-up devices. For instance, devices consisting of off-the-shelf capillaries
95 embedded within an easy-to-fabricate T-junction manifold have been previously employed to produce
96 microbubbles (Parhizkar, et al. 2013, Parhizkar, et al. 2015, Parhizkar, et al. 2014). Parhizkar *et al.*
97 employed capillaries with inner diameter in the range 100-200 μm , and investigated the effect of
98 varying the viscosity and surface tension of the liquid phase on microbubble size and size distribution
99 (Parhizkar, et al. 2013). They showed that bubble diameter could be reduced down to approximately
100 half of the capillary diameter, but that the minimum bubble diameter ($\sim 50 \mu\text{m}$) was still too large for
101 clinical use. Moreover, addition of viscosity-enhancers should be considered carefully in clinical
102 formulations.

103 **C. Multi-stage and hybrid devices for microbubble production**

104 Approaches relying on a two-stages microbubble production process have also been proposed,
105 whereby larger precursor bubbles are produced in a first step, and their size is subsequently reduced
106 down to clinically-applicable levels in a second step. Given the larger size of the precursor bubbles, it
107 is possible to utilise channels of larger dimensions compared to microfluidic devices relying on a
108 single-step microbubble production process. For example, Gnyawali *et al.* employed a 20 μm flow
109 focusing orifice to produce bubbles of $\sim 100 \mu\text{m}$ diameter, which were then conveyed through a
110 serpentine shaped channel around which a negative pressure was applied (Gnyawali, et al. 2017). As
111 the bubbles traversed this channel, the generated vacuum drove gas out of the bubbles, which in turn
112 shrunk down to a useable clinical range of 1-7 μm in diameter. Microbubbles were stable at
113 atmospheric pressure for at least 25 minutes, although their acoustic response or handling stability
114 were not reported. Additionally, as each large precursor bubble generates only a single microbubble,
115 the microbubble concentration in the end-product is likely to be low. Finally, the gas within the
116 microbubbles may be irreversibly lost without some form of scavenging, which may be problematic if
117 an expensive and/or polluting gas (e.g., sulphur hexafluoride) is employed as the microbubble core.

118 A further two-step approach that has been explored for microbubble production relies on the
119 sonication of precursor bubbles induced by low-frequency ultrasound waves. Its implementation has
120 been reported in a study by Chen *et al.* Large gas bubbles were firstly conveyed through an 860 μm
121 (inner diameter) polyethylene tube to form a gas-in-liquid slug flow regime, with the fluid containing
122 $\sim 100\text{-}300$ nm diameter ethyl cellulose particles. They subsequently travelled in front of a 20 kHz
123 ultrasonic horn, externally coupled to the capillary, causing cavitation to occur at the interface between
124 the gas bubbles and the particle-rich fluid. Cavitation resulted in the formation of microbubbles, which
125 were stabilised by adsorption of the nanoparticles onto the gas-liquid interface. microbubble size
126 dispersity could be reduced by increasing the sonication power, but it still encompassed a broad
127 diameter range (i.e. from approximately 5 to 60 μm) (Chen, et al. 2014). The microbubble size
128 distribution with the lowest dispersity had a peak diameter of ~ 20 μm , which is beyond the accepted
129 limit for intravenous administration. Furthermore, the fluid temperature was observed to increase up
130 to 80°C within 7 minutes of sonication, which may hinder the applicability of this method to the
131 production of microbubbles loaded with bioactive compounds. However, compared to the approach
132 by (Gnyawali, et al. 2017), this method enables production of multiple microbubbles from a single
133 precursor bubble and therefore presents greater scalability potential. A summary of the microbubble
134 sizes, polydispersity and production rates reported for published device is shown in Table 1 to show
135 the key advances in size control and/or production rate.

136 Ohl *et al.* developed a T-junction microfluidic device coupled with a piezoelectric element, to
137 investigate the behaviour of a gas-liquid interface exposed to ~ 100 kHz continuous ultrasound waves.
138 It was shown that these interfaces develop standing surface waves, the amplitude of which depended
139 upon the driving acoustic intensity (Ohl, et al. 2010). Pronounced crests formed at sufficiently high
140 intensity, resulting in the entrapment of small bubbles between neighbouring and coalescing crests.
141 These bubbles in turn underwent inertial cavitation and fragmentation; however, their size was not

142 fully characterised. The study thus demonstrates that it is possible to design a microfluidic system
 143 coupled with an ultrasound source, in which the amplitude of the ultrasound wave can modulate the
 144 surface oscillation of larger precursor bubbles, potentially leading to the formation of smaller
 145 micrometre-scale bubbles. It also demonstrates that, by designing the system to maximise the acoustic
 146 energy within the microfluidic channels, heat losses can be minimised. A similar approach however,
 147 has not yet been investigated for the production of coated microbubbles with clinically relevant
 148 characteristics.

149 The aim of the present study was therefore to determine whether a hybrid sonication-
 150 microfluidic (or ‘sonofluidic’) device could be used to produce microbubbles in the 1-2 μm diameter
 151 range with a clinically acceptable size distribution (all bubbles $< 5 \mu\text{m}$), and with production rates and
 152 microbubble stability comparable to those of batch methods.

Approximate MB mean diameter (μm)	Polydispersity index immediately after manufacture	Maximum MB Production Rate (MBs/sec)	Primary MB shell constituent	Reference
5	$< 2\%$	10^6	Phospholipid	Hettiarachchi <i>et al.</i> 2007
4	$< 2\%$	10^6	Phospholipid and protein	Seo <i>et al.</i> 2010
2	10-50%	10^6	Phospholipid	Peyman <i>et al.</i> 2012
5	Not cited	Not cited	Phospholipid	Gnyawali <i>et al.</i> 2017
2.5	3%	10^6	Phospholipid	van Elburg <i>et al.</i> 2021

153
 154 Table 1: Summary of the microbubble sizes, polydispersity and production rates reported for
 155 selected published microfluidic devices.
 156

157

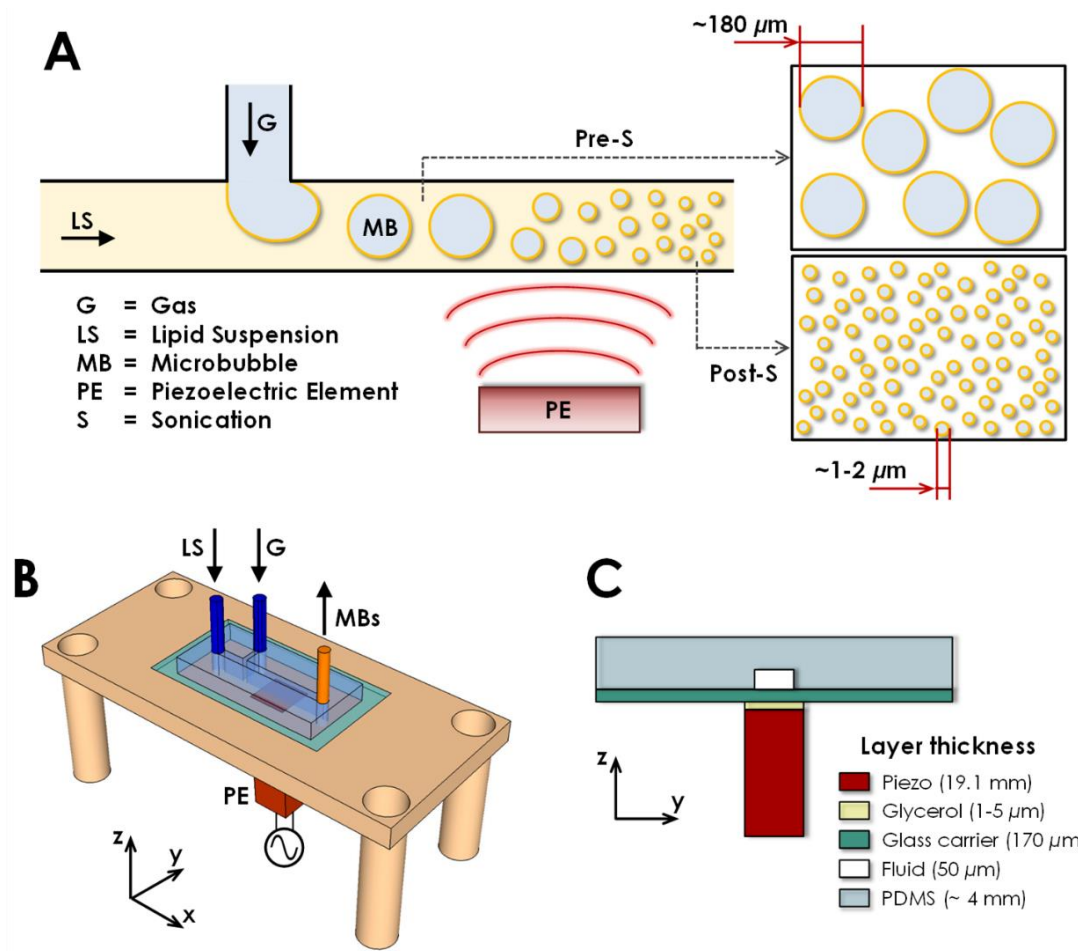
158

159 **II. MATERIALS AND METHODS**

160 **A. Sonofluidic device for microbubble production**

161 **1. *Operating principle***

162 The sonofluidic device developed in this study relies on a two-stages process to produce coated
163 gas microbubbles, as illustrated in Figure 1A. In the first stage, relatively large bubbles ($\sim 180 \mu\text{m}$ in
164 diameter) with a narrow size distribution are generated from a simple T-junction channel architecture
165 by a hydrodynamic pinch-off mechanism. In the second stage, bubbles are exposed to low-frequency
166 ultrasound from a piezoelectric transducer coupled with the exit channel from the T-junction, which
167 causes the large bubbles to ‘release’ a population of smaller microbubbles (with mean diameter
168 typically of $\sim 1\text{-}2 \mu\text{m}$). This operating principle was selected on the basis of the following postulated
169 benefits compared to more conventional microfluidic-based approaches: (i) multiple microbubbles
170 can be produced from a single precursor bubble to enhance production rates; (ii) high acoustic energy
171 density can be generated within the microfluidic channel whilst minimising heat losses, which enables
172 both effective absorption of coating material at the gas-liquid interface as well as incorporation of
173 thermolabile bioactive compounds; (iii) given the relatively large size of the precursor bubbles, the
174 microfluidic channels can be manufactured using cost-effective, easy-to-perform, and scalable
175 techniques, and devices can be operated at larger volumetric flow rates; and (iv) devices can be
176 potentially integrated with detection systems for in-line quantification of microbubble size
177 distribution.



178

179 FIG. 1. (A) Schematic depiction of the operating principle governing microbubble generation within
 180 the sonofluidic device. Larger bubbles ($\sim 180 \mu\text{m}$ in diameter) are produced using a T-junction
 181 microfluidic architecture and exposed to a low frequency (in the range 71-73 kHz) ultrasound field,
 182 causing the precursor bubbles to release smaller microbubbles (with mean diameter of $\sim 1-2 \mu\text{m}$). (B)
 183 Schematic depiction of the overall sonofluidic device assembly. The microfluidic T-junction device
 184 was positioned on to a custom-built holder, and coupled with a piezoelectric element (PE) generating
 185 the ultrasound field. Flows of gas (G) and a lipid suspension (LS) were conveyed through the device
 186 inlets, while the generated microbubble (microbubble) suspension was collected from the outlet. (C)
 187 Cross-sectional view of the constitutive layers of the sonofluidic device, with indicated the
 188 corresponding thickness for each layer. The ultrasound field was generated by a 19.1 mm thick

189 piezoelectric element (piezo), and travelled through a 0.17 mm thick glass carrier layer that was coupled
190 to the piezoelectric transducer *via* a thin layer of glycerol (estimated thickness: 1 – 5 μm). It then
191 propagated into the fluid layer of the microfluidic device (thickness: 50 μm), and subsequently through
192 a \sim 4 mm thick layer of PDMS.

193 **2. Device design, manufacturing and assembly**

194 The microfluidic T-junction comprised two inlet and one outlet channels, with a rectangular cross-
195 section (width \times depth) of 250 $\mu\text{m} \times$ 50 μm (liquid suspension inlet and outlet) and 125 $\mu\text{m} \times$ 50 μm
196 (gas inlet). This channel architecture was cast in poly(dimethylsiloxane) (PDMS, SylgardTM 184, Dow
197 Inc., Michigan, USA) using a combined micromilling-replica moulding ($\mu\text{Mi-REM}$) technique
198 described previously (Carugo, et al. 2016). Briefly, the channel architecture was micromilled into a
199 poly(methyl methacrylate) (PMMA, theplasticshop.co.uk, Coventry, UK) block to form a negative
200 mould. A positive mould was manufactured by coating the milled PMMA mould with a bi-component
201 epoxy adhesive (1:1 weight ratio between components, Yellow Dual Cartridge, RS Components Ltd.,
202 Corby, UK), which was then degassed by vacuum to remove entrapped air bubbles and left to cure at
203 room temperature. After curing, the positive epoxy mould was removed from the PMMA block, and
204 a 10:1 (w/w) mixture of PDMS and curing agent was poured over it and degassed for approximately
205 30 minutes to remove entrapped air bubbles. The PDMS layer was then cured overnight at room
206 temperature. To complete the manufacturing process, the PDMS layer was removed from the positive
207 epoxy mould and the patterned surface was activated by plasma treatment (using a plasma cleaner
208 ATTO, Diener electronic GmbH, Ebhausen, Germany) along with a 74.00 mm \times 49.00 mm \times 0.17
209 mm (length \times width \times thickness) glass layer (Logitech, Glasgow, UK). After \sim 60-80 s of treatment,
210 the PDMS layer was pressed firmly against the glass, and the assembly was heat treated on a hotplate
211 set to 100°C for 10 minutes to achieve effective bonding between glass and PDMS. To create inlet
212 and outlet ports for the gas and liquid flows, 1/16” polyether ether ketone (PEEK) rods were glued

213 by low-cost solvent-free glue (Pritt, Henkel Ltd., Herts., UK) onto the epoxy layer before PDMS
214 pouring. The rods were then removed upon PDMS curing, prior to plasma treatment. After bonding
215 to the glass surface, short segments of 3/32" OD Tygon® tubing (Cole-Parmer Instrument Co. Ltd.,
216 London, UK) were inserted into the ports to act as connectors for 1/16" OD tubing. These were
217 connected to relevant syringes or gas circuits by 18G blunt needles (Sigma Aldrich, Gillingham, UK).

218 The PDMS device was then placed on to a custom holder (manufactured from polyoxymethylene),
219 which contained a recess, in which the microfluidic device was positioned, and a central cut out
220 window through which an ultrasound transducer was placed for coupling with the glass layer of the
221 device (Figure 1B). Reversible coupling was achieved using a small volume of glycerol, which allowed
222 for easy removal or replacement of the microfluidic device when required. The thin glass layer thus
223 acted as an effective carrier for the ultrasound wave generated by the transducer, which was positioned
224 5 mm away from the junction between inlet channels. PDMS has a comparable characteristic acoustic
225 impedance to the one of water (Carugo, et al. 2015, Leibacher, et al. 2014), it was therefore anticipated
226 that ultrasound reflections at the liquid-PDMS interface would be minimised. The ultrasound
227 transducer consisted of a single piezoelectric element (9.0 mm × 9.0 mm × 19.1 mm, Pz26, Meggitt
228 PLC, UK) with a fundamental thickness resonance frequency of 69 kHz. Figure 1C shows a cross-
229 sectional view of the constitutive layers of the sonofluidic device, in the region where the transducer
230 is coupled with the glass layer, with the corresponding thickness values indicated for each layer.

231 ***3. Electronic components and ultrasound actuation methods***

232 The transducer was driven in continuous mode by a 55 dB RF power amplifier (1040L, E&I,
233 Rochester, NY, USA) fed from a signal generator (Agilent 33220A, Keysight Technologies, Santa
234 Rosa, USA). Two different actuation methods were used in the present study, namely single frequency
235 (SF) and frequency modulation (FM). In the latter method, a linear frequency sweeping was applied,

236 and the effects of varying both the frequency range and sweep period (or duration) on microbubble
237 characteristics were investigated.

238 **B. Microbubble Formulations**

239 Phospholipids were selected as the primary microbubble coating material in this study, as they are the
240 most commonly used shell constituent in commercial contrast agents (e.g., SonoVue®, Sonazoid®
241 and Definity®) (Frinking, et al. 2020). The lipids 1,2-distearoyl-sn-glycero-3-phosphocholine (DSPC,
242 850365), 1,2-dipalmitoyl-sn-glycero-3-phosphocholine (DPPC, 850355) 1,2-Dipalmitoyl-sn-glycero-
243 3-phosphatidic acid sodium salt (DPPA, 830855), 1,2-distearoyl-sn-glycero-3-phosphoethanolamine-
244 N-[methoxy(polyethylene glycol)-5000] (DSPE-mPEG5000, 880220) and 1,2-dipalmitoyl-sn-glycero-
245 3-phospho-(1'-rac-glycerol) (DPPG, 840455) were purchased as a 25 mg/mL solution in chloroform
246 or powders from Avanti Polar Lipids, Inc. (Alabaster, AL, USA). Two different formulations of the
247 microbubble shell were investigated, corresponding to: (i) a mixture of DSPC and polyoxyethylene
248 (40) stearate (PEG-40S), which is a composition widely used in research settings (Borden, et al. 2005,
249 Owen, et al. 2018); and (ii) a mixture of DPPC, DSPE-mPEG5000, and DPPA, which is comparable
250 to the formulation of the clinically approved Definity® microbubbles (Lantheus Medical Imaging,
251 MA, USA) (Segers, et al. 2017). In the first formulation, DSPC (25 mg/mL in chloroform) and PEG-
252 40S (10 mg/mL in chloroform) were mixed in a glass vial to form a chloroform solution at a molar
253 ratio of 9:1, respectively. In the second formulation, DPPC (25 mg/mL in chloroform), DSPE-
254 mPEG5000 (25 mg/mL in chloroform) and DPPA (1 mg/mL in a chloroform, methanol and water
255 mix) were mixed in a glass vial to a 20 mg total of lipid constituents at a molar ratio of 8:1:1,
256 respectively. Chloroform solutions were covered with perforated Parafilm® (Bemis Company, Inc.,
257 Neenah, WI, USA) and allowed to evaporate overnight to form a homogenous lipid film. 10 mL Milli-
258 Q water (Merck Millipore, Watford, UK) or a water, glycerol and propylene glycol mixture (80:10:10
259 v/v respectively) was added to the DSPC or Definity®-like lipid films, respectively. In the case of the

260 DSPC-based formulation, three different DSPC concentrations in the final suspension were
261 investigated, corresponding to 2, 4 and 6 mg/mL, to assess whether lipid concentration had an effect
262 on the characteristics of microbubbles produced using the sonofluidic device. The lipids were
263 resuspended into the solvent by stirring at 100°C on a magnetic stirrer hotplate for a minimum of 30
264 minutes. They were then homogeneously dispersed within the solution by sonication for
265 approximately 2.5 minutes using a micro-sonicator tip fully immersed in the solution at a power setting
266 of 2 to 3 (Microson XL 2000, QSonica, Newtown, CT, USA).

267 **C. Experimental procedures**

268 Microbubbles produced using the sonofluidic device were compared with those produced by
269 conventional sonication in terms of their size, stability, and concentration. In addition, the effect of
270 changing the sonofluidic device driving ultrasound parameters was investigated, and performance
271 consistency across multiple devices was assessed. Finally, different lipid formulations and
272 concentrations were investigated.

273 **1. Production of lipid microbubbles by conventional sonication**

274 After resuspension and dispersion of lipids into the solvent, the sonicator tip was placed at the
275 air-liquid interface and the headspace in the vial filled with nitrogen gas. The solution was sonicated
276 under constant nitrogen flow for 30 seconds at a power setting of 14, to form a suspension of
277 microbubbles. The suspension was left to cool to room temperature over 5 minutes. Typically, clinical
278 microbubble formulations use heavy gases such as perfluorobutane or sulfur hexafluoride, but to
279 facilitate a large number of experiments, nitrogen (supplied by BOC Gases, Guildford, UK) was used
280 in this study.

281 **2. Production of lipid microbubbles using the sonofluidic device**

282 The device channels were flushed with ethanol and deionised water multiple times prior to use.
283 The resuspended, fully dispersed lipid solution was transferred to a 10 mL syringe and connected to
284 the liquid inlet port of the device. The gas inlet was connected to a nitrogen cylinder *via* a dual stage
285 regulator with cut-off valve and an inline electronic pressure manometer (2023P Digitron, Elektron
286 Technology, Cambridge, UK). A syringe pump (World Precision Instruments Inc., Florida, USA) was
287 used to vary lipid flow rates into the device, whilst gas pressure control was supplied by the regulator.
288 The device was run for one minute to establish a stable ‘pinch-off’ regime at the T-junction, indicated
289 by the appearance of a steady stream of large bubbles. This regime was achieved at a volumetric flow
290 rate of the lipid suspension of 0.5 mL/min and a nitrogen inlet pressure of 37 kPa. The mean diameter
291 of the produced bubbles was approximately 180 μm , determined through optical microscopy of the
292 collected bubble suspension (please see below). Upon formation of a steady bubble flow, the
293 ultrasound transducer was actuated, which resulted in the production of smaller microbubbles. These
294 were also collected from the outlet tube for microscopic analysis.

295 **3. Microbubble concentration, size and stability analysis**

296 Sonicated microbubbles were homogeneously dispersed by gentle manual agitation of the vial, and
297 10 μL of the suspension were loaded on a coverslip-covered haemocytometer *via* a pipette. The
298 continuous-flow format of the sonofluidic device meant that the outlet tube could be directly
299 connected to the hemocytometer chamber. Microbubbles were imaged using a brightfield microscope
300 (Leica Microsystems GmbH, Wetzlar, Germany), and images were acquired using a digital camera
301 (MicroPublisher 3.3 RTV, QImaging, Surrey, Canada). A 4 \times or 40 \times objective was used for imaging
302 the larger precursor bubbles ($\sim 180 \mu\text{m}$ mean diameter) and smaller microbubbles ($\sim 1\text{-}10 \mu\text{m}$
303 diameter), respectively. Microbubble size and concentration were determined using a purpose-written
304 image processing program in MATLAB (The Mathworks Inc., Natick, MA, USA), as previously
305 described in Sennoga *et al.* (Sennoga, et al. 2012). A minimum of twenty images were analysed for each

306 sample. For stability analysis, microbubble size and concentration were measured as described every
307 10 minutes from the same sample. This was repeated three times using a fresh bubble suspension
308 created from a new lipid film each time. The average microbubble mean diameter values reported in
309 this manuscript are accompanied by the corresponding average standard deviation of the diameter
310 distribution, which provides a quantification of microbubble size dispersity. Experiments were
311 performed at the ambient room temperature ($\sim 18\text{-}22^\circ\text{C}$) and pressure. The microscope lamp was
312 switched off in between measurements to avoid excessive heating of the sample, and the coverslip
313 was left in place on the haemocytometer throughout.

314 **4. Optimisation of sonofluidic device operating parameters**

315 The effects of varying the sonofluidic device operating ultrasound parameters on microbubble
316 production rate and size distribution were investigated. Parameters included the acoustic energy (e.g.,
317 by changing the input driving voltage to the amplifier in the range 300 – 900 mV), the frequency value
318 in single frequency operation mode (in the range 67 – 76 kHz), and the sweep frequency range
319 (between 69 kHz and 73 kHz) and period (in the range 1 – 1000 ms) in frequency modulation mode.
320 Optimal operating parameters were identified, which provided the greatest production rate whilst
321 retaining a clinically relevant mean microbubble diameter (of $\sim 1\text{-}2\ \mu\text{m}$) and a low size dispersity.

322 **5. Reproducibility of the sonofluidic device**

323 To test the performance reproducibility of the sonofluidic device, three devices of the same design
324 were constructed and run at the optimal ultrasound settings. Microbubbles in these experiments were
325 produced using three independent lipid suspensions of DSPC:PEG40s (9:1 molar ratio).

326 **D. Sonofluidic device for scaled-up microbubble production**

327 A modified design of the sonofluidic device was developed to perform a preliminary investigation
328 of whether microbubble production rates could be scaled-up by increasing both the microfluidic

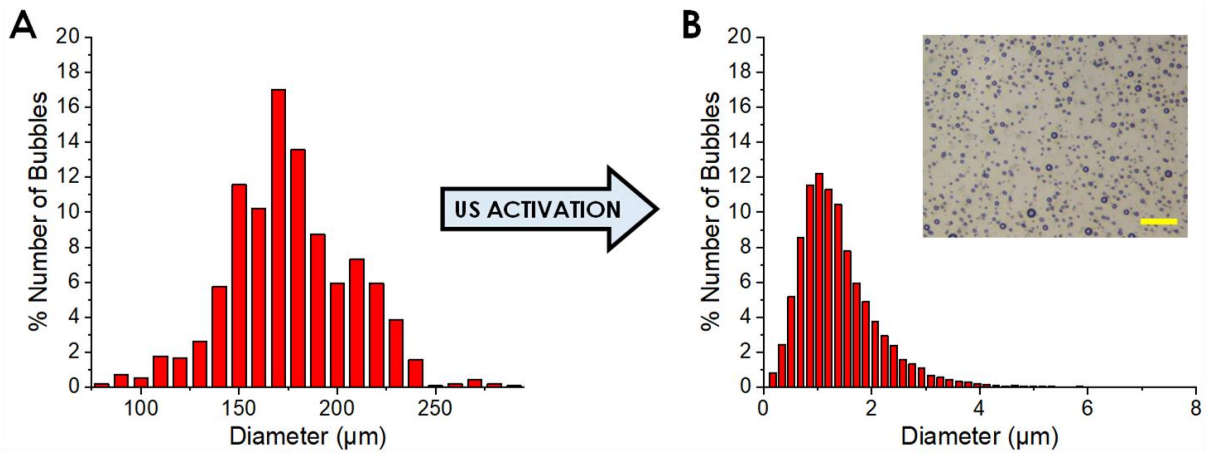
329 device cross-sectional dimensions (and thus the operating flow rates) and the ultrasound field intensity.
330 This scaled-up sonofluidic device was designed, manufactured, and operated following the same
331 principles and procedures reported above. The ultrasound transducer was changed to a 60 kHz
332 piezoelectric element (maximum power: 30 W, PZT-4, Beijing Ultrasonic, China), and the glass layer
333 to a thicker 75 mm \times 25 mm \times 1 mm (length \times width \times thickness) slide to effectively sustain the
334 greater levels of ultrasound-induced strain. The fluidic channels of the T-junction architecture had
335 increased cross-sectional dimensions (width \times thickness) of 1.0 \times 0.1 mm (liquid suspension inlet and
336 exit channels) and 0.5 \times 0.1 mm (gas inlet channel). In the experiments using this scaled-up device,
337 the ultrasonic transducer was driven at a peak-to-peak voltage (post amplification) of 200 V and the
338 driving frequency was linearly swept between 60 and 62 kHz. These ultrasound settings were
339 maintained constant throughout the experiments, while the volumetric flow rate of the lipid
340 suspension was increased from 5 to 35 mL/min. The gas inlet pressure was manually adjusted as the
341 liquid flow rate was increased, in order to maintain a stable stream of precursor bubbles forming at
342 the junction between inlet channels. The lipid suspension in these experiments comprised DSPC and
343 PEG40S at a molar ratio of 9:1, suspended in a water, glycerol and propylene glycol mixture (80:10:10
344 v/v respectively). The microbubbles size and concentration were determined by optical microscopy,
345 following the protocol described above.

346 III. RESULTS AND DISCUSSION

347 A. Optimisation of sonofluidic device operating parameters

348 Figure 2 shows representative diameter distributions of phospholipid-coated (DSPC:PEG40S)
349 precursor bubbles (i.e., not exposed to the ultrasound field) and the microbubbles generated upon
350 activation of the piezoelectric transducer. Precursor bubbles formed at the T-junction by a pinch-off
351 mechanism, and had a mean diameter of 181 μ m and standard deviation of the distribution of 34 μ m
352 (Figure 2A), corresponding to a polydispersity index (PDI) of 0.035. Once exposed to the ultrasound

353 field, they formed microbubbles with a size distribution having mean diameter of $1.45 \mu\text{m}$ and
354 standard deviation of $0.76 \mu\text{m}$ (Figure 2B), corresponding to a PDI of 0.27.



355
356 FIG. 2. Representative percentage weighted size distributions of (A) bubbles prior to activation of the
357 piezoelectric transducer (based on 20 images of ~ 1000 bubbles), and (B) microbubbles generated
358 upon activation of the ultrasound field (based on 30 images of ~ 13000 bubbles). The inset shows a
359 representative microscope image of microbubbles produced using the sonofluidic device (scale bar:
360 $10 \mu\text{m}$).

361 In order to determine the optimal operating parameters for the device, the driving ultrasound
362 frequency, amplitude, and frequency sweep settings were all varied. In a first series of experiments,
363 the transducer was driven in SF mode, and the effect of varying the ultrasound frequency was
364 investigated. Frequency values evaluated were equal to 67, 69, 71, 73 and 76 kHz, at a constant pre-
365 amplifier input voltage of 900 mV (see Figure 3A). It was found that increasing the ultrasound
366 frequency from 67 kHz to 69 kHz resulted in an increase in microbubble concentration (from $0.43 \pm$
367 0.06×10^8 microbubbles/mL to $1.05 \pm 0.33 \times 10^8$ microbubbles/mL) and a slight decrease in
368 microbubble mean diameter and size dispersity (from $2.19 \pm 1.28 \mu\text{m}$ to $1.90 \pm 1.02 \mu\text{m}$). A similar
369 trend was observed when the frequency was further increased from 69 kHz to 71 kHz (microbubble
370 concentration: $1.99 \pm 0.25 \times 10^8$ microbubbles/mL; mean microbubble diameter: $1.56 \pm 0.83 \mu\text{m}$).

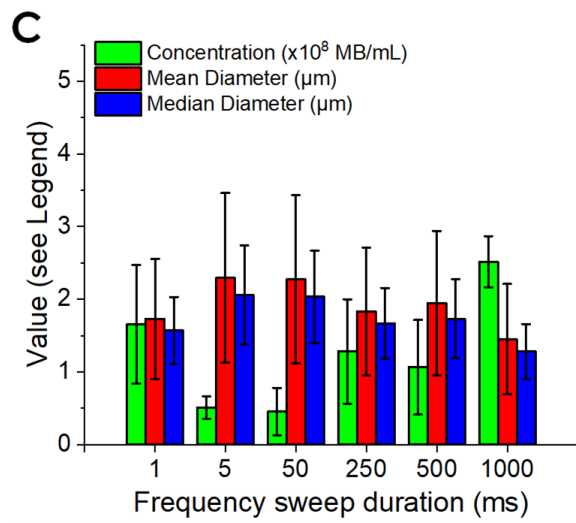
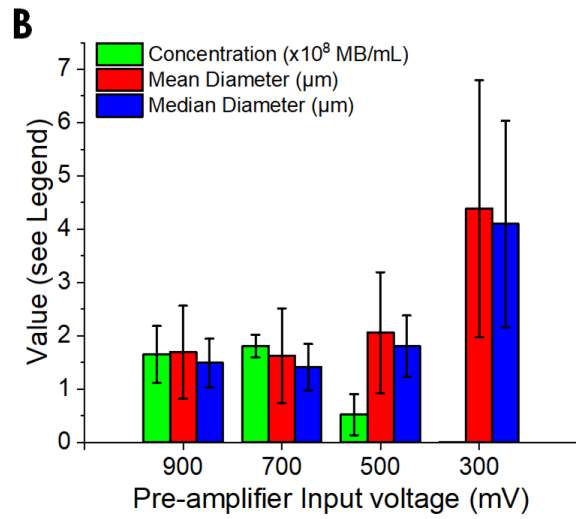
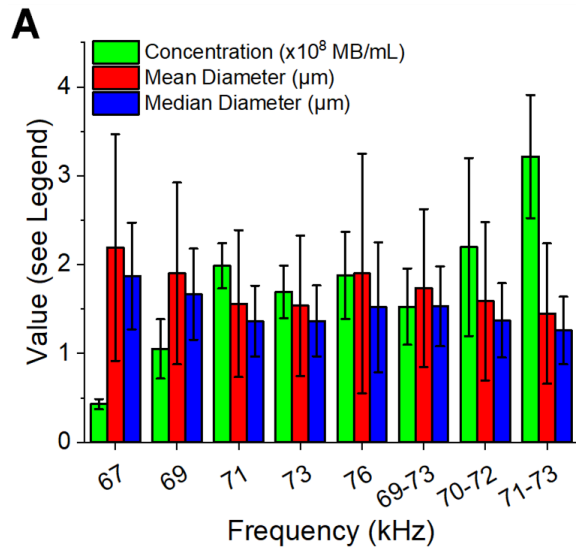
371 However, microbubbles produced at 73 kHz had comparable mean diameter and size dispersity (1.54
372 $\pm 0.79 \mu\text{m}$) to those produced at 71 kHz, and only a slightly reduced concentration ($1.69 \pm 0.29 \times 10^8$
373 microbubbles/mL). Further increasing the driving frequency to 76 kHz caused a marginal increase in
374 both microbubble size (mean diameter: $1.90 \pm 1.35 \mu\text{m}$) and concentration ($1.88 \pm 0.49 \times 10^8$
375 microbubbles/mL), but this was accompanied by an increase in the corresponding standard
376 deviations. In a second series of experiments, the transducer was operated by applying a linear
377 frequency modulation over a range of driving frequencies that excluded those values that resulted
378 either in the lowest microbubble production rate (67 kHz) or the greatest variability in microbubble
379 concentration and size (76 kHz). The sweep frequency ranges investigated were 69-73 kHz, 70-72
380 kHz, and 71-73 kHz, at a constant sweep period of 50 ms. Among the different modulation regimes
381 evaluated, the 71-73 kHz sweep range resulted in the greatest microbubble concentration (3.22 ± 0.69
382 $\times 10^8$ microbubbles/mL), corresponding to a production rate of approximately 2.7×10^6
383 microbubbles/s, and a clinically viable mean diameter of $1.45 \pm 0.79 \mu\text{m}$, and was thus selected as the
384 preferred operating condition for subsequent tests. Operating the device in frequency sweeping also
385 brings with it additional benefits, such as reduced temperature sensitivity, less requirements for
386 controlling the ultrasound frequency (i.e., through automated frequency tracking methods), and
387 potentially greater uniformity of the acoustic field within the fluid layer, as previously reported for
388 other acoustofluidic devices (Carugo, et al. 2014, Manneberg, et al. 2009) . It should be noted that the
389 optimal driving frequencies did not include the nominal resonance frequency of the piezoelectric
390 element (67 kHz), which could be due to the effect of coupling the transducer with the microfluidic
391 device structure. In some cases, it could also be observed that the produced microbubbles weren't
392 efficiently released from the device, potentially due to the 'trapping' effect of acoustic radiation forces.
393 Future studies could thus evaluate a wider range of combinations of driving frequencies and inlet

394 volumetric flow rates, as well as the applicability of a pulsed ultrasound mode, to further optimise
395 microbubbles production rate.

396 The effect of varying the amplitude of the operating ultrasound wave was subsequently
397 investigated (see Figure 3B), at a frequency sweep range of 71-73 kHz and period of 50 ms. By varying
398 the pre-amplifier input voltage from 300 mV to 500 mV resulted in a significant increase in
399 microbubble concentration (from $0.82 \pm 0.16 \times 10^6$ to $0.52 \pm 0.39 \times 10^8$ microbubbles/mL) and a
400 reduction in microbubble mean diameter and corresponding standard deviation (from $4.39 \pm 2.41 \mu\text{m}$
401 to $2.06 \pm 1.13 \mu\text{m}$). When the input voltage was further increased to 700 mV, it was again observed
402 an increase in microbubble concentration ($1.81 \pm 0.21 \times 10^8$ microbubbles/mL) and a corresponding
403 reduction in both microbubble mean diameter and standard deviation ($1.63 \pm 0.89 \mu\text{m}$). The observed
404 effect of the ultrasound intensity on microbubble characteristics may be due to the fact that the gas-
405 liquid interface of precursor bubbles underwent oscillations of greater amplitude at the higher
406 ultrasound intensities, which resulted in more frequent entrapments and subsequent fragmentation
407 events of smaller microbubbles, consistently with the observations by Ohl and co-authors (Ohl, et al.
408 2010). The relationship between driving voltage and microbubble properties was however non-linear,
409 and a further increase in the pre-amplifier input voltage (up to 900 mV) did not cause significant
410 changes in both microbubble concentration ($1.65 \pm 0.54 \times 10^8$ microbubbles/mL) and size ($1.69 \pm$
411 $0.87 \mu\text{m}$). Whilst input voltages of 700 mV and 900 mV led to comparable microbubble characteristics,
412 the latter was selected as the preferred operating voltage in order to accommodate for potential
413 reductions in the acoustic energy within the device, i.e., due to fluctuations in environmental
414 temperature, variabilities in the manufacturing process, or other factors. Results also suggest that
415 varying the input voltage to the sonofluidic device may be an effective way of tuning the microbubble
416 mean diameter, although careful consideration should be given to the corresponding reduction in
417 microbubble concentration.

418 Subsequently, the effect of varying the sweep duration (or period) was also investigated (see
419 Figure 3C). The transducer was driven at a pre-amplifier input voltage of 900 mV, and the frequency
420 was linearly swept between 71 and 73 kHz over a period of either 1, 5, 50, 250, 500, and 1000 ms.
421 Interestingly, the highest microbubble concentrations were generated at 1 ms and 1000 ms sweep
422 duration ($1.66 \pm 0.81 \times 10^8$ microbubbles/mL and $2.52 \pm 0.35 \times 10^8$ microbubbles/mL, respectively),
423 with a corresponding microbubble diameter of $1.73 \pm 0.83 \mu\text{m}$ (1 ms) and $1.45 \pm 0.76 \mu\text{m}$ (1000 ms).
424 Although there was no obvious relationship between microbubble characteristics and sweep period,
425 the greater production rate at the lowest sweep period (1 ms) may be due to the fact that precursor
426 bubbles were exposed to the optimal operating frequency for a longer period of time as they travelled
427 above the transducer, when compared to greater sweep periods (5 - 500 ms). The reasons behind
428 increased microbubble production rates at the highest sweep period (1000 ms) are not fully understood
429 yet, and merit further investigations. Previous studies using acoustofluidic resonators have shown that
430 frequency modulation can induce an oscillatory translational motion on particles or biological cells
431 suspended in a microfluidic cavity, and that the amplitude of oscillation scales with the sweep duration
432 (Ankrett, et al. 2013, Jonnalagadda, et al. 2018). It may thus be hypothesised that this enhanced
433 oscillatory motion may promote release of microbubbles from the gas-liquid interface of precursor
434 bubbles, overall resulting in greater microbubble concentrations in the end-product. Future studies
435 using ultra-high speed microscopy will be performed to gain a more pervasive understanding of the
436 effect of sweep duration on precursor bubble behaviour and microbubbles production mechanism.

437 Overall, the sonofluidic device operating parameters were chosen to be: a 71-73 kHz frequency
438 sweep over 1000 ms, at an input pre-amplification voltage of 900 mV, producing microbubbles of
439 mean diameter of $\sim 1.45 \mu\text{m}$ and $\text{PDI} = 0.27$, at a production rate in the order of $\sim 2 \times 10^6$
440 microbubbles/s.



441

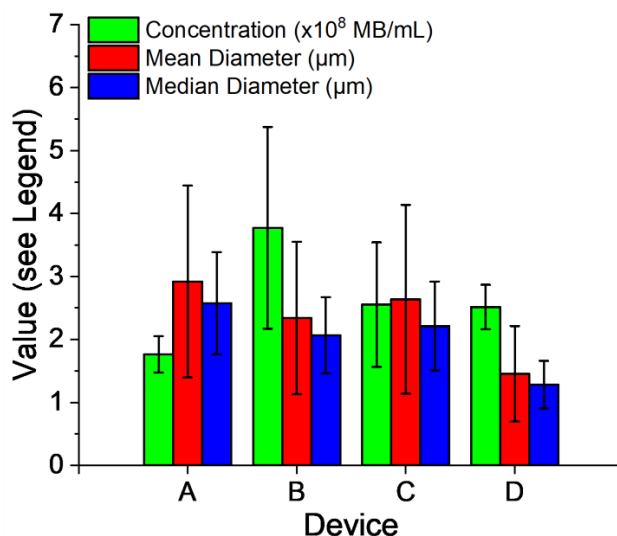
442

443 FIG. 3. (A) Effect of driving acoustic frequency on microbubble properties. The graph shows the
444 population statistics of microbubbles generated at varying acoustic frequencies, at both single
445 frequency and frequency modulation actuation modes. The piezoelectric transducer was operated at a
446 pre-amplifier input voltage of 900 mV. The sweeping frequency groups (69-73, 70-72 and 71-73 kHz)
447 used a linear frequency sweep over 50 ms. The optimum waveform frequency was chosen as a 71-73
448 kHz frequency sweep. $n = 3$ per frequency. The error bars indicate one standard deviation. (B) Effect
449 of acoustic power on microbubble properties. The graph shows the population statistics of
450 microbubbles generated at varying acoustic pre-amplifier input voltage. The piezoelectric transducer
451 was run using a frequency sweep of 71-73 kHz over 50 ms. The optimum waveform pre-amplifier
452 input voltage was chosen as 900 mV, although 700 mV provided microbubbles of comparable
453 characteristics and would also be useable. $n = 3$ per input voltage. (C) The graph shows the effect of
454 frequency sweep duration on microbubble properties. Population statistics of microbubbles generated
455 at varying acoustic frequency sweep duration. The piezoelectric transducer was run using a frequency
456 sweep of 71-73 kHz at pre-amplifier input voltage of 900 mV. The optimum waveform sweep duration
457 was chosen as 1000 ms. $n = 3$ per frequency sweep, except 50 ms which is $n = 2$.

458 **B. Sonofluidic device performance reproducibility**

459 Three additional replicas of the microfluidic device were manufactured and run using the same
460 piezoelectric transducer, to investigate performance reproducibility across different devices. Notably,
461 the adopted reversible acoustic coupling enabled efficient removal and replacement of the microfluidic
462 device units from the custom-built holder. Devices were all operated using a frequency sweep of 71-
463 73 kHz over 1000 ms, at a pre-amplifier input voltage of 900 mV. The size and concentration of
464 microbubbles produced with each device replica are reported in Figure 4 (Devices A, B, and C),
465 together with those of the device previously utilised during performance optimisation tests (Device C,
466 Figure 3C). The microbubble concentration varied in the range $1.76 - 3.77 \times 10^8$ microbubbles/mL,

467 with an average between devices of $2.65 \pm 0.83 \times 10^8$ microbubbles/mL. The mean microbubble
468 diameter varied in the range 1.45 - 2.92 μm , and the average between devices was $2.34 \pm 0.64 \mu\text{m}$.

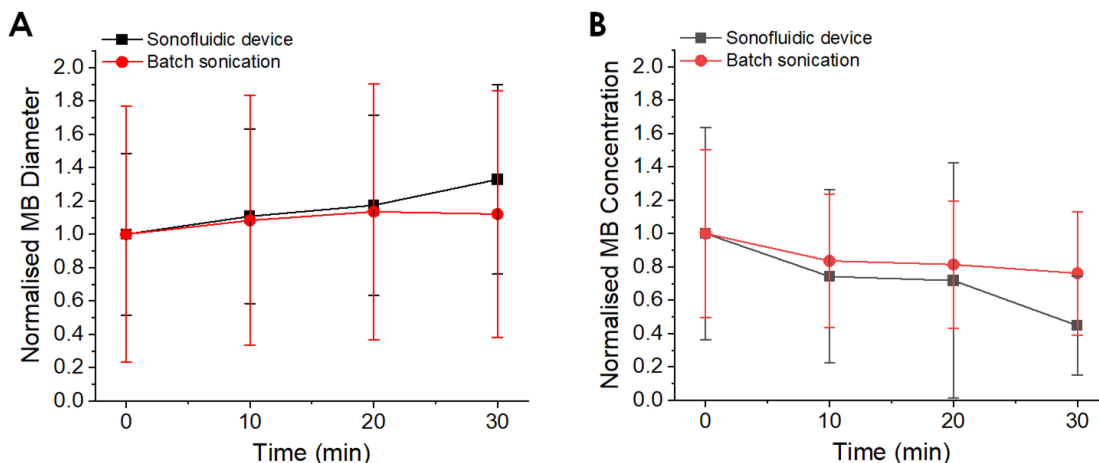


469
470 FIG. 4. Reproducibility of sonofluidic device performance. The graph shows the population statistics
471 of microbubbles generated at a frequency sweep in the range 71-73 kHz over 1000 ms, at a pre-
472 amplifier input voltage of 900 mV. In each group of experiments, a different microfluidic device was
473 employed. The lipid formulation used was a 2 mg/mL DSPC:PEG40S. $n = 3$ per device.

474 Differences in performance between devices could be potentially attributed to discrepancies in the
475 positioning of the piezoelectric element relative to the microfluidic channel architecture. This could
476 be due to the nature of the manufacturing process, whereby the PDMS layer was manually bonded to
477 the glass substrate. There may have also been differences in the thickness of the glycerol coupling
478 layer between devices, which may have affected the acoustic energy field within the microfluidic
479 channels. Moreover, using a commercial transducer with built-in case, may reduce performance
480 sensitivity to changes in the environmental conditions. Overall, considering the cost-effective and
481 easy-to-perform nature of the manufacturing method employed in this study, all sonofluidic device
482 replicas were capable of producing phospholipid-shelled microbubbles at rates $>10^6$ microbubbles/s
483 and with a clinically acceptable diameter.

484 **C. Comparison with conventional batch sonication**

485 DSPC:PEG40S (9:1) microbubbles were prepared both by batch sonication and using the
486 sonofluidic device, and their size distribution and concentration were monitored over 30 minutes in a
487 hemocytometer. The normalised average microbubble concentration and mean diameter are reported
488 in Figures 5A and 5B, respectively. The microbubble suspensions produced by batch sonication had
489 a larger initial mean diameter ($2.65 \mu\text{m}$) compared to those produced using the sonofluidic device
490 ($1.75 \mu\text{m}$), and also contained microbubbles with diameter $>10 \mu\text{m}$. The concentration of
491 microbubbles produced by batch sonication was greater than the ones produced using the sonofluidic
492 device, but of the same order of magnitude (4.34×10^8 microbubbles/mL *vs.* 1.71×10^8
493 microbubbles/mL).



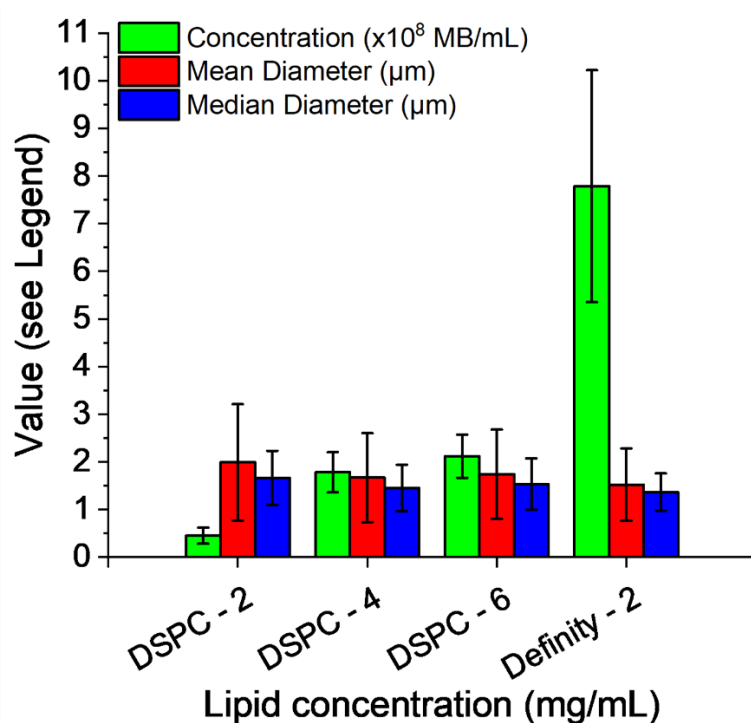
494
495 FIG. 5. Comparison of the stability of microbubbles produced by batch sonication and the sonofluidic
496 device. Changes in (A) normalised mean diameter and (B) normalised concentration of microbubbles
497 produced by sonication (red circles and line) and the sonofluidic device (black squares and line) over
498 30 minutes, measured from bright field microscope images. The sonofluidic device was operated using
499 a frequency sweep in the range 71-73 kHz over 1000 ms, at a pre-amplifier input voltage of 900 mV.
500 $n = 3$ per production method.

501 As shown in Figure 5, both types of microbubble underwent a comparable gradual decrease in
502 concentration and increase in mean diameter over a period of 30 minutes. A two-sample *t*-test was
503 performed on data pairs, and there were no statistically significant differences in microbubble
504 properties between the two production techniques, suggesting that microbubbles produced using the
505 sonofluidic device have comparable stability to those produced using conventional batch sonication.

506 **D. Modification of microbubble formulation**

507 The total lipid concentration of DSPC:PEG40S was varied in the range 2-6 mg/mL, to determine
508 whether the amount of phospholipid had an effect on the characteristics of microbubbles produced
509 using the sonofluidic device (see Figure 6). It was found that increasing the lipid concentration from
510 2 to 6 mg/mL increased microbubble concentration from $0.45 \pm 0.17 \times 10^8$ microbubbles/mL to
511 $2.12 \pm 0.45 \times 10^8$ microbubbles/mL, likely due to the greater number density of phospholipid
512 molecules readily available to stabilise the gas-liquid interface of the forming microbubbles. The
513 increase in microbubble concentration was however less pronounced when the lipid concentration
514 was varied from 4 to 6 mg/mL ($1.78 \pm 0.42 \times 10^8$ microbubbles/mL *vs.* $2.12 \pm 0.45 \times 10^8$
515 microbubbles/mL). The mean microbubble diameter did not show significant changes as a function
516 of the total lipid concentration, and was in the range 1.67-1.99 μm . An alternative formulation, similar
517 to that used in the commercial agent Definity®, was also tested using a 2 mg/mL total lipid
518 concentration. microbubble shell constituents in this formulation were DPPC, DSPE-mPEG5000,
519 and DPPA (at a molar ratio of 8:1:1). Unlike the DSPC:PEG40S microbubbles, the resuspension
520 solvent was a more viscous solution of water, glycerol, and propylene glycol. The average microbubble
521 concentration with this formulation was significantly greater than for DSPC:PEG40S, and equal to
522 $7.79 \pm 2.43 \times 10^8$ microbubbles/mL (corresponding to an average production rate of 6.5×10^6
523 microbubbles/s). The mean microbubble diameter was slightly reduced when compared to the
524 DSPC:PEG40s formulation with the same total lipid concentration (1.52 μm *vs.* 1.99 μm). These

525 observations are consistent with previous studies that reported an increase in microbubble
 526 concentration for DPPC-based formulations containing both glycerol and propylene glycol, and
 527 produced by mechanical agitation (Daeichin, et al. 2016). This is likely due to the reduced diffusivity
 528 of gas in the suspending medium as compared to saline, inhibiting microbubble destruction during
 529 processing; propylene glycol is also an effective de-foaming agent and this may help to promote
 530 formation of microbubbles over foam. A previous study by Parhizkar *et al.* also reported on an inverse
 531 relationship between diameter and medium viscosity, for microbubbles produced in a capillary
 532 embedded T-junction device (Parhizkar, et al. 2015). Moreover, the greater viscosity of the suspension
 533 medium in the Definity®-like formulation likely increased the overall microbubble lifetime.

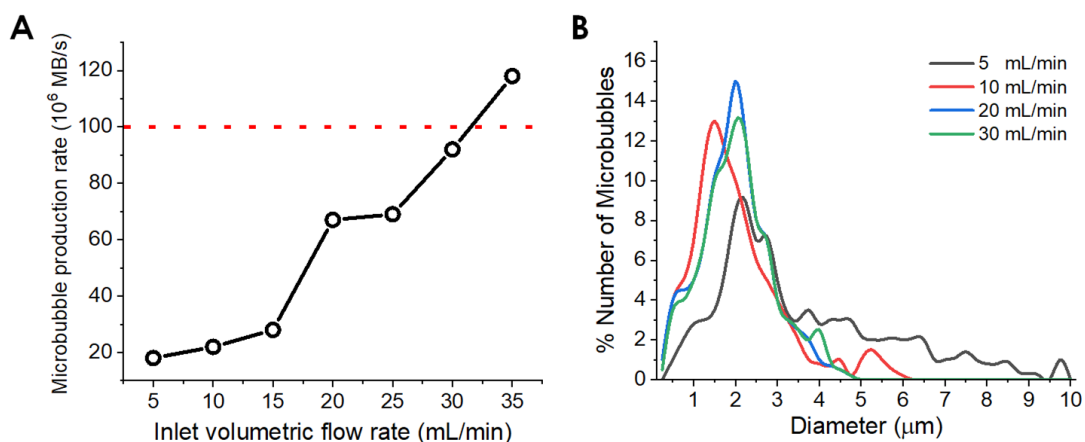


534
 535 FIG. 6. Effect of total lipid concentration and formulation on the characteristics of microbubbles
 536 produced using the sonofluidic device. The graph shows the population statistics of microbubbles
 537 generated at a frequency sweep in the range 71-73 kHz over 1000 ms, at a pre-amplifier input voltage
 538 of 900 mV and using different lipid concentrations of DSPC:PEG40S and a Definity®-like

539 formulation. Optimisation of lipid concentration and formulation can improve microbubble
540 production rates. $n = 3$ per formulation.

541 E. Demonstration of scaled-up microbubble production

542 Microbubbles were produced using the sonofluidic device described in section II.D, which
543 consisted of a scaled-up microfluidic channel architecture operated at greater volumetric flow rates
544 and driving acoustic power. The lipid suspension in these experiments comprised DSPC and PEG40S
545 at a molar ratio of 9:1, suspended in a water, glycerol and propylene glycol mixture (80:10:10 v/v
546 respectively). Notably, the microbubble production rate for this device directly correlated with the
547 inlet flow rate, and increased from 0.18×10^8 microbubbles/s (at 5 mL/min) up to a maximum of
548 1.18×10^8 microbubbles/s (at 35 mL/min) for a single device, as shown in Figure 7A.



549
550 FIG. 7. (A) Microbubble production rate as a function of the inlet volumetric flow rate of the
551 phospholipid suspension, obtained using the scaled-up sonofluidic device (driven using a 30 W
552 transducer). The dotted red horizontal line corresponds to a production rate of 100 millions of
553 microbubbles per second. (B) microbubbles size distribution at four different inlet volumetric flow
554 rates. The lipid suspension in these experiments comprised DSPC and PEG40S at a molar ratio of
555 9:1, and the suspension medium was a mixture of water, glycerol and propylene glycol (80:10:10 v/v).

556 This corresponds to an increase of 1 to 2 orders of magnitude compared to the sonofluidic device
557 configuration described above and other methods that have been published (Table 1). Volumetric
558 flow rates >35 mL/min resulted in delamination of the PDMS from the glass substrate, and
559 subsequent leakage. However, greater production rates may be achievable by improving the PDMS-
560 glass bonding strength through optimisation of the plasma treatment process. As shown in Figure 7B,
561 the microbubble size dispersity reduced with increasing the volumetric flow rate from 5 mL/min to
562 20 mL/min; however, it remained substantially unchanged at flow rates ≥ 20 mL/min. The greater
563 size dispersity at the lower flow rates requires further investigations, but may be due to the increased
564 transit time of precursor bubbles across the ultrasound field that may have potentially resulted in
565 enhanced microbubble fragmentation and coalescence.

566 **F. Limitations and future development for microbubble production**

567 The results from this study demonstrate the feasibility of the proposed sonofluidic method as a
568 means of producing microbubbles with a clinically relevant composition and size distribution, and in
569 a continuous-flow format. The mechanism of microbubble formation was not explicitly investigated.
570 It is hypothesised that standing surface waves were established at the gas-liquid interface of the larger
571 precursor bubbles, and that the resulting surface oscillations led to the entrapment and ‘release’ of
572 smaller microbubbles, consistent with the observations reported by Ohl *et al.* (Ohl, et al. 2010). Further
573 work is required to test this hypothesis using high speed imaging as the device architecture and
574 microbubble formulation are different.

575 To the best of the authors’ knowledge, this is the first study reporting on the use of this approach
576 to produce microbubbles stabilised with clinically relevant formulations of coating material, including
577 a mimic of the clinically approved contrast agent Definity®. Compared to conventional batch
578 sonication or other two-stage methods relying on ultrasound exposure of precursor bubbles (Chen, et
579 al. 2014), the microbubbles produced using the sonofluidic device could be directly administered

580 intravenously without the need for post-production fractionation or centrifugation processes that are
581 typically required to eliminate microbubbles with diameter $>10\ \mu\text{m}$. It will be necessary, however, to
582 confirm that the coating properties and acoustic response of the microbubbles are also comparable to
583 those of microbubbles produced via sonication.

584 The proposed sonofluidic strategy can produce microbubbles at rates of 10^8 per second using a
585 single channel, which is significantly greater than that achievable with conventional microfluidic
586 approaches and comparable to batch sonication. Production rates of $>10^9$ microbubbles per second
587 could easily be achieved through parallel actuation of multiple channels within a single platform; and
588 even higher rates using multiple devices. A further important point is that the risk of sample
589 contamination from erosion of the sonicator tip is also removed, as there is no direct contact between
590 the microbubble suspension and the ultrasound transducer as in batch sonication. This may be
591 advantageous for good manufacturing practice (GMP) compliance, and for producing microbubble
592 formulations loaded with bioactive compounds. The risk of clogging associated with conventional
593 microfluidic devices is also minimized and encapsulation efficiency expected to be significantly higher
594 than for conventional emulsification. This will likely be beneficial for the preparation of multi-
595 component bubbles, e.g. surface functionalised with targeting ligands or containing solid particles, for
596 which clogging is a greater risk. It would also be comparatively simple to add a secondary channel to
597 the device to facilitate subsequent reaction with a functional component. e.g. microbubbles could be
598 generated with a biotinylated lipid and then functionalised by exposing them to an avidin
599 functionalised drug molecule or targeting ligand. Production of functionalized microbubbles has yet
600 to be demonstrated, however, and this will be evaluated in future investigations, together with a
601 broader range of clinically applicable microbubble shell constituents.

602 There are other aspects of the developed system that also require improvement. These include (i)
603 the repeatability of the microfluidic device manufacturing process, and particularly of the relative

604 positioning of the PDMS and glass layers, (ii) the repeatability of the coupling process between the
605 piezoelectric element and glass carrier, and (iii) the use of scalable and high volume capacity fluid
606 supply units (e.g., pressurised reservoirs) as an alternative to syringe pumps. The results of this study
607 also suggest that varying the input acoustic intensity may provide an effective means of controlling
608 the microbubble size, although this may also result in a change in microbubble concentration. Future
609 studies will investigate whether operating the device over a broader range of ultrasound frequencies
610 (i.e., including harmonics of the transducer fundamental resonance frequency) would offer a method
611 for tuning microbubble size and achieving a narrower size distribution.

612

613 **IV. CONCLUSIONS**

614 The feasibility of producing microbubbles with clinically relevant size (1-2 μm) and
615 composition using a sonofluidic device was demonstrated. The microbubble diameter, concentration
616 and stability were comparable with those achieved with batch sonication, but with a narrower size
617 distribution and importantly no microbubbles larger than $<5 \mu\text{m}$ in diameter. This removes the need
618 for post-production fractionation. Production rates of $>10^8$ microbubbles per second were achieved
619 using a single device. These are comparable with production rates associated with batch sonication,
620 but the risk of contamination and/or degradation of sensitive components is removed. The device
621 can also be operated continuously, reducing the risk of batch to batch variation. Further work is
622 needed to elucidate the mechanism of microbubble formation within the device and to characterize
623 the microbubble surface and acoustic properties.

624 **ACKNOWLEDGEMENTS**

625 This work was supported by the Institute of Engineering and Technology (AF Harvey Prize)
626 and the Engineering and Physical Sciences Research Council (grants EP/I021795/1 and

627 EP/L025825/1). The authors gratefully acknowledge the help of Mr James Fisk in the University of
628 Oxford workshop for assistance in device manufacturing.

629 REFERENCES

- 630 Al-Jawadi S, Thakur SS. Ultrasound-responsive lipid microbubbles for drug delivery: A review of
631 preparation techniques to optimise formulation size, stability and drug loading. *International*
632 *journal of pharmaceutics* 2020;119559.
- 633 Alter J, Sennoga CA, Lopes D, Eckersley RJ, Wells DJ. Microbubble stability is a major determinant of the
634 efficiency of ultrasound and microbubble mediated in vivo gene transfer. *Ultrasound in*
635 *medicine & biology* 2009; 35:976-84.
- 636 Ankrett DN, Carugo D, Lei J, Glynne-Jones P, Townsend PA, Zhang X, Hill M. The effect of ultrasound-
637 related stimuli on cell viability in microfluidic channels. *Journal of nanobiotechnology* 2013;
638 11:1-5.
- 639 Borden MA, Kruse DE, Caskey CF, Zhao S, Dayton PA, Ferrara KW. Influence of lipid shell physicochemical
640 properties on ultrasound-induced microbubble destruction. *IEEE transactions on ultrasonics,*
641 *ferroelectrics, and frequency control* 2005; 52:1992-2002.
- 642 Browning RJ, Aron M, Booth A, Rademeyer P, Wing S, Brans V, Shrivastava S, Carugo D, Stride E. Spectral
643 Imaging for Microbubble Characterization. *Langmuir* 2019; 36:609-17.
- 644 Carugo D, Lee JY, Pora A, Browning RJ, Capretto L, Nastruzzi C, Stride E. Facile and cost-effective
645 production of microscale PDMS architectures using a combined micromilling-replica moulding
646 (μ Mi-REM) technique. *Biomedical microdevices* 2016; 18:4.
- 647 Carugo D, Octon T, Messaoudi W, Fisher AL, Carboni M, Harris NR, Hill M, Glynne-Jones P. A thin-
648 reflector microfluidic resonator for continuous-flow concentration of microorganisms: a new
649 approach to water quality analysis using acoustofluidics. *Lab on a Chip* 2014; 14:3830-42.
- 650 Carugo D, Owen J, Crake C, Lee JY, Stride E. Biologically and acoustically compatible chamber for
651 studying ultrasound-mediated delivery of therapeutic compounds. *Ultrasound in medicine &*
652 *biology* 2015; 41:1927-37.
- 653 Castro-Hernández E, Van Hove W, Lohse D, Gordillo JM. Microbubble generation in a co-flow device
654 operated in a new regime. *Lab on a Chip* 2011; 11:2023-29.
- 655 Chen H, Li J, Zhou W, Pelan EG, Stoyanov SD, Arnaudov LN, Stone HA. Sonication–Microfluidics for
656 Fabrication of Nanoparticle-Stabilized Microbubbles. *Langmuir* 2014; 30:4262-66.
- 657 Daeichin V, van Rooij T, Skachkov I, Ergin B, Specht PA, Lima A, Ince C, Bosch JG, van der Steen AF, de
658 Jong N. Microbubble composition and preparation for high-frequency contrast-enhanced
659 ultrasound imaging: in vitro and in vivo evaluation. *IEEE transactions on ultrasonics,*
660 *ferroelectrics, and frequency control* 2016; 64:555-67.
- 661 Dewitte H, Roovers S, De Smedt SC, Lentacker I. Enhancing nucleic acid delivery with ultrasound and
662 microbubbles. *Nanotechnology for Nucleic Acid Delivery*: Springer, 2019. 241-51.
- 663 Dhanaliwala AH, Chen JL, Wang S, Hossack JA. Liquid flooded flow-focusing microfluidic device for in situ
664 generation of monodisperse microbubbles. *Microfluidics and nanofluidics* 2013; 14:457-67.
- 665 Dollet B, van Hove W, Raven J-P, Marmottant P, Versluis M. Role of the channel geometry on the
666 bubble pinch-off in flow-focusing devices. *Physical review letters* 2008; 100:034504.
- 667 Ferrara K, Pollard R, Borden M. Ultrasound microbubble contrast agents: fundamentals and application
668 to gene and drug delivery. *Annu. Rev. Biomed. Eng.* 2007; 9:415-47.
- 669 Feshitan JA, Chen CC, Kwan JJ, Borden MA. Microbubble size isolation by differential centrifugation.
670 *Journal of colloid and interface science* 2009; 329:316-24.

671 Frinking P, Segers T, Luan Y, Tranquart F. Three decades of ultrasound contrast agents: a review of the
672 past, present and future improvements. *Ultrasound in medicine & biology* 2020; 46:892-908.

673 Garg S, Thomas AA, Borden MA. The effect of lipid monolayer in-plane rigidity on in vivo microbubble
674 circulation persistence. *Biomaterials* 2013; 34:6862-70.

675 Garstecki P, Fuerstman MJ, Stone HA, Whitesides GM. Formation of droplets and bubbles in a
676 microfluidic T-junction—scaling and mechanism of break-up. *Lab on a Chip* 2006; 6:437-46.

677 Gnyawali V, Moon B-U, Kieda J, Karshafian R, Kolios MC, Tsai SS. Honey, I shrunk the bubbles:
678 microfluidic vacuum shrinkage of lipid-stabilized microbubbles. *Soft Matter* 2017; 13:4011-16.

679 Hettiarachchi K, Talu E, Longo ML, Dayton PA, Lee AP. On-chip generation of microbubbles as a practical
680 technology for manufacturing contrast agents for ultrasonic imaging. *Lab on a Chip* 2007; 7:463-
681 68.

682 Hosny NA, Mohamedi G, Rademeyer P, Owen J, Wu Y, Tang M-X, Eckersley RJ, Stride E, Kuimova MK.
683 Mapping microbubble viscosity using fluorescence lifetime imaging of molecular rotors.
684 *Proceedings of the National Academy of Sciences* 2013; 110:9225-30.

685 Jiang X, Zhang Y, Edirisinghe M, Parhizkar M. Combining microfluidic devices with coarse capillaries to
686 reduce the size of monodisperse microbubbles. *RSC advances* 2016; 6:63568-77.

687 Jonnalagadda US, Hill M, Messaoudi W, Cook RB, Oreffo RO, Glynne-Jones P, Tare RS. Acoustically
688 modulated biomechanical stimulation for human cartilage tissue engineering. *Lab on a Chip*
689 2018; 18:473-85.

690 Kooiman K, Vos HJ, Versluis M, de Jong N. Acoustic behavior of microbubbles and implications for drug
691 delivery. *Advanced drug delivery reviews* 2014; 72:28-48.

692 Leibacher I, Schatzer S, Dual J. Impedance matched channel walls in acoustofluidic systems. *Lab on a*
693 *Chip* 2014; 14:463-70.

694 Manneberg O, Vanherberghen B, Önfelt B, Wiklund M. Flow-free transport of cells in microchannels by
695 frequency-modulated ultrasound. *Lab on a Chip* 2009; 9:833-37.

696 Ohl S-W, Ow DS-W, Klaseboer E, Wong VV, Camattari A, Ohl C-D. Creation of cavitation activity in a
697 microfluidic device through acoustically driven capillary waves. *Lab on a Chip* 2010; 10:1848-55.

698 Owen J, Kamila S, Shrivastava S, Carugo D, Bernardino de la Serna J, Mannaris C, Pereno V, Browning R,
699 Beguin E, McHale AP. The Role of PEG-40-stearate in the Production, Morphology, and Stability
700 of Microbubbles. *Langmuir* 2018; 35:10014-24.

701 Pahlavan AA, Stone HA, McKinley GH, Juanes R. Restoring universality to the pinch-off of a bubble.
702 *Proceedings of the National Academy of Sciences* 2019; 116:13780-84.

703 Parhizkar M, Edirisinghe M, Stride E. Effect of operating conditions and liquid physical properties on the
704 size of monodisperse microbubbles produced in a capillary embedded T-junction device.
705 *Microfluidics and nanofluidics* 2013; 14:797-808.

706 Parhizkar M, Edirisinghe M, Stride E. The effect of surfactant type and concentration on the size and
707 stability of microbubbles produced in a capillary embedded T-junction device. *Rsc Advances*
708 2015; 5:10751-62.

709 Parhizkar M, Stride E, Edirisinghe M. Preparation of monodisperse microbubbles using an integrated
710 embedded capillary T-junction with electrohydrodynamic focusing. *Lab on a Chip* 2014; 14:2437-
711 46.

712 Peyman SA, Abou-Saleh RH, McLaughlan JR, Ingram N, Johnson BR, Critchley K, Freear S, Evans JA,
713 Markham AF, Coletta PL. Expanding 3D geometry for enhanced on-chip microbubble production
714 and single step formation of liposome modified microbubbles. *Lab on a Chip* 2012; 12:4544-52.

715 Rademeyer P, Carugo D, Lee JY, Stride E. Microfluidic system for high throughput characterisation of
716 echogenic particles. *Lab on a Chip* 2015; 15:417-28.

717 Rickel JR, Dixon AJ, Klibanov AL, Hossack JA. A flow focusing microfluidic device with an integrated
718 Coulter particle counter for production, counting and size characterization of monodisperse
719 microbubbles. *Lab on a Chip* 2018; 18:2653-64.

720 Segers T, Gaud E, Casqueiro G, Lassus A, Versluis M, Frinking P. Foam-free monodisperse lipid-coated
721 ultrasound contrast agent synthesis by flow-focusing through multi-gas-component microbubble
722 stabilization. *Applied Physics Letters* 2020; 116:173701.

723 Segers T, Lohse D, Versluis M, Frinking P. Universal equations for the coalescence probability and long-
724 term size stability of phospholipid-coated monodisperse microbubbles formed by flow focusing.
725 *Langmuir* 2017; 33:10329-39.

726 Sennoga CA, Yeh JS, Alter J, Stride E, Nihoyannopoulos P, Seddon JM, Haskard DO, Hajnal JV, Tang M-X,
727 Eckersley RJ. Evaluation of methods for sizing and counting of ultrasound contrast agents.
728 *Ultrasound in medicine & biology* 2012; 38:834-45.

729 Seo M, Gorelikov I, Williams R, Matsuura N. Microfluidic Assembly of Monodisperse, Nanoparticle-
730 Incorporated Perfluorocarbon Microbubbles for Medical Imaging and Therapy. *Langmuir* 2010;
731 26:13855-60.

732 Sirsi S, Feshitan J, Kwan J, Homma S, Borden M. Effect of microbubble size on fundamental mode high
733 frequency ultrasound imaging in mice. *Ultrasound in medicine & biology* 2010; 36:935-48.

734 Stride E, Edirisinghe M. Novel microbubble preparation technologies. *Soft matter* 2008; 4:2350-59.

735 Stride E, Saffari N. Microbubble ultrasound contrast agents: a review. *Proceedings of the Institution of
736 Mechanical Engineers, Part H: Journal of Engineering in Medicine* 2003; 217:429-47.

737 Stride E, Segers T, Lajoinie G, Cherkaoui S, Bettinger T, Versluis M, Borden M. Microbubble agents: New
738 directions. *Ultrasound in medicine & biology* 2020; 46:1326-43.

739 van Elburg B, Collado-Lara G, Bruggert GW, Segers T, Versluis M, Lajoinie G. Feedback-controlled
740 microbubble generator producing one million monodisperse bubbles per second. *Rev Sci
741 Instrum* 2021; 92.

742